MSc in Photonics

Universitat Politècnica de Catalunya (UPC)
Universitat Autònoma de Barcelona (UAB)
Universitat de Barcelona (UB)
Institut de Ciències Fotòniques (ICFO)

PHOTONICS**BCN**

http://www.photonicsbcn.eu

Master in Photonics

MASTER THESIS WORK

An Optofluidic Router in a low-cost (PDMS) platform for rapid parallel sample analysis.

Jeroen Goyvaerts

Supervised by Dr. Andreu Llobera, CNM-CSIC UAB
Co-supervised by prof. Maria Garcia-Parajo, ICFO
Co-supervised by prof. Crina Cojocaru, UPC

Presented on the 9th of September 2016

Registered at

Escola Tècnica Superior d'Enginyeria de Telecomunicació de Barcelona

Lab on a Chip

PAPER

Cite this: DOI: 10.1039/xxxxxxxxxx

An optofluidic router in a low-cost (PDMS) platform for rapid parallel sample analysis.†

Jeroen Goyvaerts,*[a,b] Tobias N. Ackermann,[b] Erica Alvarez,[b] Jordi Vila-Planas,[b] and Andreu Llobera [b]

Received Date
Accepted Date

DOI: 10.1039/xxxxxxxxxx

www.rsc.org/journalname

Optofluidic system for (bio)chemical applications are becoming more demanding in terms of number of control points, number of light sources and readout equipment. So far, most of these systems require several light sources/detectors for suitable performance, increasing their complexity and cost. In this work, we present an easily integrated, fluidically controlled optical router that facilitates coupling of several light sources or detectors. By using PDMS mirrors and phaseguides, the switching liquid is guided and pinned in desired angles, so that the incident light undergoes total internal reflection and can be reflected towards the output channels without any movable parts. The developed router presents ideal performance for lab on a chip applications, achieving switching frequencies between 0.07 ± 0.025 and 4 ± 2 Hz, depending on the flow rate of the switching liquid. The cross-talk levels are at 20 dB from channel output power to static noise level. With the use of parabolic mirrors, channel coupling efficiencies decrease just 2.38 dBm over four channels. The dynamic switching noise reduces the cross-talk levels by 2-5 dB, depending on the incorporation of ink-apertures. The insertion loss of these devices ranges from 17.34 to 25.42 dB. These results prove the viability of the fluidically controlled router in the low-cost PDMS platform. The intended goal of this work has been to simplify and speed up parallel sample analysis with the router integrated into a multiple path photonic component on a single chip. Development on this front is ongoing to rapidly measure methadone concentrations on chip.

1 Introduction

Nowadays, lab on a chip (LOC) applications are becoming extremely sophisticated analysis[1] platforms requiring statistical analysis and multiple control points[2,3] in order to achieve reliable analysis performance[4]. As a sign of technological matureness, raw samples can now be purified, split on multiple aliquots and transported, via an arbitrary complex microfluidic network, to a specific region of the LoC where the measurement of the analyte of interest takes place. The paradigm in this approach is that from an analytical perspective, the number of divisions of a given sample should be the highest to be able to detect either the largest number of analytes or a specific analyte with high accuracy through parallel analysis. Conversely, this parallelization exponentially increases the readout complexity, since it requires to have at least one transducer for each measurement region/aliqout. The challenge in LoC technology is how to perform such measurements without compromising either sample sterility or the technological viability of the LoC itself while holding the low-cost assumption.

Equally important is defining the most appropriate transducer to transform this biorecognition event into a quantifiable signal. In this group, different transduction mechanisms, such as electrochemical[5] and optical[6], have already been integrated into LoCs. Among them, the latter have demonstrated to be one of the most sensitive analytical and selective detection methods for analysis[7]. The transference of this know-how from the macro- to the microscale has already been demonstrated with the so-called photonic lab on a chip (PhLoC)[8]. Micro-optical elements, such as micro-lenses and mirrors[9], can be implemented in the vicinity of a microfluidic network to provide the entire system with the required optical readout. Even highly promising, PhLoC generally require two fiber optics, one coupled to the light emitter and another to the detector for each aliquot. As the number of such systems increases (or the number of detection regions in a given PhLoC), errors due to inadequate fiber optics positioning also in-

[a] Universitat Polytècnica de Cataluyna (UPC), Campus Nord, Calle Jordi Girona 1-3, 08034 Barcelona, Spain.
[b] Institut de Microelectrònica de Barcelona (IMB-CNM, CSIC), Campus UAB, 08193 Bellaterra, Spain. E-mail: andreu.llobera@imb-cnm.csic.es

† Electronic Supplementary Information (ESI) available, X files: detailed jpg of design, mkv-files on filling & emptying of the router, supporting simulation results and more. See DOI: 10.1039/b000000x/

crease, making the PhLoC concept to have low yield if the number of aliquots is N>4. Here, the most suitable approach would be an integrated optical router suitable to provide single input/single output readout, and then being able to sequentially interrogate each aliquot.

Hitherto, most of the commercial optical routers are conceived for telecommunication applications, which results in a very narrow working wavelength range (centered at $\lambda = 1550$ nm), being then unsuitable for the broadband requests of optical sensing. For wavelengths in the visible range, bulky commercial optical routers are available. Moreover, these commercial routers are expensive and difficult to integrate in LoC systems.

Regarding optofluidical routers, Fouquet et al. reported a 4x4 planar optofluidic router with fast switching frequencies of 1 kHz [10]. The working principle was based on total internal reflection at air bubbles generated by thermal actuators that were fabricated on a separate system, increasing the costs and technological complexity. Groisman et al. reported a 1x4 router based on refractive index (RI) changes of a liquid over a diffraction grating [11]. This optofluidic router had a switching frequency of 18.2 Hz. Nonetheless, RI changes require four liquids with different RI to allow the optical switching. Besides, the optical router worked in an out of plane configuration, complicating the integration in LOC applications. Recently an optofluidic router based on electrowetting on dielectrics (EWOD) has been presented [12]. EWOD actuators are used to precisely control a water/oil interface which acts as a mirror when the TIR conditions are fulfilled. Due to EWOD actuators, LOC fabrication complexity, cost and response time increase, achieving switching frequencies at or below 0.6 Hz. The cross-talk levels recorded below 10 dB extinction ratio.

All reported optical routers require non-standard technologies, dramatically increasing fabrication costs and time and thus preventing their integration in optofluidic systems. This work presents, for the very first time, a phaseguide-based optofluidic router, which is technologically compatible with the PhLoC technology, since only Polydimethylsiloxane (PDMS) and re-usable liquids are used as its main constituents. The router has been designed, fabricated and characterized.

2 Design & Operation

The router that is introduced here is designed according to figures 1-(a) and 1-(b). The router design is patterned in PDMS and bonded to a glass plate substrate. It has one input (Ch0) and four output (Ch1 to Ch4 from right to left) optical channels, thus forming a 1X4 router. Each optical channel comprises of a self-alignment microchannel and a cylindrical dual-microlens system that also acts as the fiber stopping interface. The self-alignment microchannel allows the fiber optics to be aligned with the optical axis of the microlenses. The design of the channel is optimized to facilitate fiber insertion with a 300 μm wide opening and periodical constrictions to ensure mechanical stability that end in a final constriction width of similar size as the inserted fiber (125 μm). The microlenses at channel Ch0 are designed to collimate the light as much as possible, while the lenses at the output channels are designed to focus and match the angular acceptance angle of the fibers (0.22 NA).

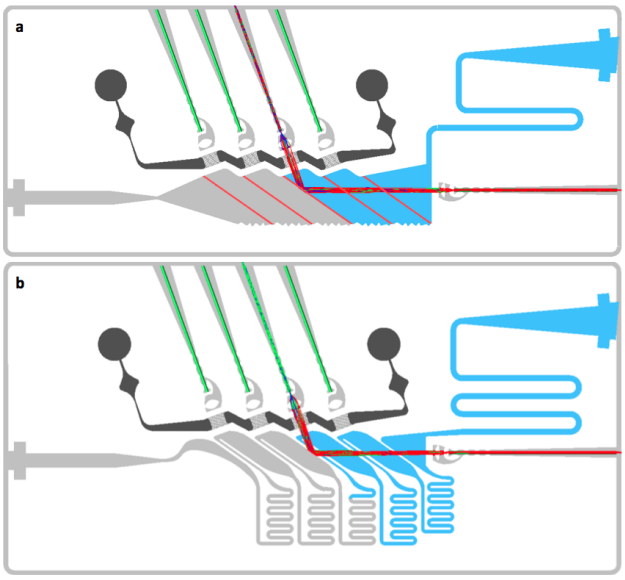

Fig. 1 *TracePro simulations of the two design concepts of the router. The switching liquid is shown in blue, with the optical fibers in green and the ink-aperture is illustrated in black. (a) shows the pressure-driven router where the phaseguides are indicated in red and form partial-PDMS mirrors. The liquid enters from the top-right inlet and fills the microchamber along the phaseguide before hopping over to the next chamber. (b) gives the continuous flow router where a meander structure acts as a time-delay structure between the channel allocations. The liquid enters the chamber from the bottom right corner and fills up until the top left corner, after which it is guided toward the bottom, into the next meander.*

The PDMS mirrors operate on controlled total internal reflection (TIR). At angles above 45 °, the total internal reflection occurs between the PDMS phaseguide and the air backside. TIR also occurs at the liquid-air interface, depending on the driving liquid. For water, with $n_{H_2O} = 1.33$, TIR occurs just below 49 °. For very incident angles, $\alpha > 70°$, TIR occurs at the front-interface between the PDMS phaseguide and in this case water. The front-side TIR can not be lifted, creating permanent leakage into the channel. The mirror orientation α is this limited between $50 - 70°$. In order to reduce the design footprint, and thus the associated optical losses due to lack of vertical confinement, α is set at 55 °.

$$\theta_{crit,mirror} = sin^{-1}(1/n_{PDMS}) = 45.1715° \quad (1)$$

$$\theta_{crit,liquid} = sin^{-1}(1/n_{H_2O}) = 48.7535° \quad (2)$$

Fluidically, the router can be envisaged as sequential microchambers to sequentially redirect the light into the channels. There are two ways to control the switching mechanism: the first being a pressure driven router shown in 1-(a), and the second being a continuous-flow router shown in 1-(b). For the pressure-driven router, the phaseguides (red in figure 1-(a)) are designed to pin the liquid advancing meniscus and act as a partial PDMS mirror. Due to the liquid pinning, the meniscus behaves optically as a liquid-air mirror. However, due to the curvature of the meniscus, light leaks from the device. Therefore, the partial PDMS mirror has a height of 120 μm with a 10 μm gap. In this way, the con-

tribution of the liquid-air mirror is minimized by placing it away from the optical path. The light emerging from the collimating input lenses is then first reflected at the first phaseguide, which acts as the zero-output or OFF-switch in the router when the liquid is present. The light then effectively leaks away in the PDMS substrate. Upon crossing the barrier, the liquid fills the second chamber, and is pinned subsequently to the second phaseguide. Now, the TIR condition at the backside of the first phaseguide is destroyed due to the liquid presence and the light passes through the chamber towards the second phaseguide, and is then reflected at the backside interface of the second phaseguide, into the Ch1 output. Important to mention is that phaseguides are fixed elements, and hence the router has no movable parts, thus providing a mechanically robust optical router. In the continuous-flow router of figure 1-(b), there are no phaseguide (partial) mirrors. Instead, a dual-mirror configuration is placed to optimize the priming behavior of the switching liquid: the liquid enters at the bottom right corner of the microchamber in 1-(b) and is pushed towards the top left side. There, it is guided back down through the back-channel between both mirrors to the meander structure that acts as a time delay between the channels. In this configuration, the mirrors are completely sealed, eliminating the liquid-air mirror contribution. Also, a more controlled switching occurs versus the forceful pressure threshold in 1-(a). The benefit of the pressure-driven router lays in the minimal liquid volume and robust operation window.

The optofluidic has been numerically simulated using the commercial ray tracing software TracePro 7.3, for a wavelength of $\lambda = 635$ nm. Using the radiant source input mode of TracePro, between 10k to 100k rays are emitted from the front facet of a 0.22 NA input fiber of length 0.5m, traced through the system taking into account Fresnel reflections losses at the various interfaces, and the optical power at the end facet of the output fiber is detected, considering 0.22 as the NA of the output fiber. In figure 1, the ray propagation can be seen through the first two phaseguides (including the zero-phaseguide). When the liquid is pinned on the third phaseguide, light couples from Ch0 to Ch3, confirming the optical performance of the phaseguide-mirrors.

2.1 Spline-Optimized Lenses

The purpose of the spline-optimized lenses is to minimize the optical power loss in the 2D confined, lossy system. Three different lens systems have therefore been designed and categorized as collimation systems (input) or as focusing systems (output). The initial lens (bottom lens, above fiber in figure 2) acts as the fiber-stopped. The solid endpoint ensures optimal fiber-alignment in combination with the restricting undulations of the fiber-channel. Next, an air gap (dark gray) separates lens one and lens two from each system with an additional air gap at the topside of figure 2. The lens system is limited to two lenses, to minimize the size regarding dispersive losses and to minimize the Fresnel reflection losses at multiple air-PDMS interfaces.

Due to the size mismatch between the fiber core ($105\mu m$) and the lens dimensions ($600-900\mu m$), the Lensmakers' equations are no longer valid. As such, there are limited analytical tools

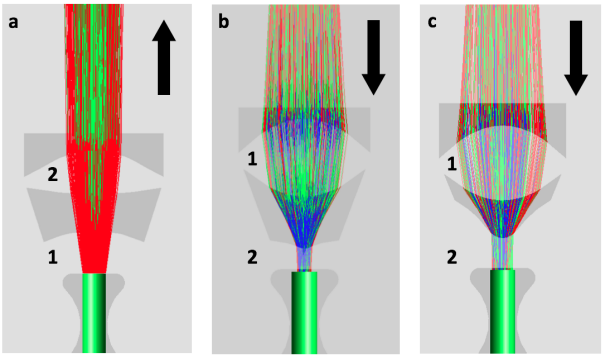

Fig. 2 *Ray tracing of the PDMS lenses in TracePro. (a) the newly spline-optimized collimation system. The other lens systems (b)-(c) are optimized for focusing the light into the output channel fibers. Spherical PDMS lens 1 focusses the light in a focal point. The secondary extreme concave lens 2 parallelizes the beam efficiently into the low aperture fiber (0.22). System (b) is optimized for small distances (<1 cm) while the system (c) is designed for larger distances (>1cm).*

that can give reliable, qualitative results. Therefore, TracePro 7.1 with a built-in optical optimization tool was used to design the lenses. The optimization covered a quarter size reduction of the lens dimensions to counteract dispersion and a conversion from spherical to spline lens-curvatures. The 3D optimization tool is based on the Downhill-simplex method, which is a commonly applied nonlinear optimization method to find extrema in a multidimensional space. The optimization function was chosen to maximum light collection at typical distances (0-2 cm) considered in the router design. While the collimation system was optimized independently, the two focusing systems were optimized in combination with the newly designed collimation system.

In order to obtain good results, a proper starting configuration is required. For the collimation system, a typical planoconvex collimates light from a point source into parallel rays. The secondary lens is convex, with soft splines curves to reduce the dispersion angle from the beam even more. Six control points were chosen, two on each interface with one near the center and the other closer to the edge of the lens. For the focusing systems, a highly convex lens is chosen to collect as much incident light as possible into the fiber. For previously mentioned reasons of practicality, only low aperture fibers with an NA of 0.22 were chosen. Therefore, the second lens is small with extreme high concave spline curvatures to reduce and match the numerical aperture of the focused light with the numerical aperture of the output fibers. Similar to the collimation system, the optimization covered six points, three per interface with one in the center and the other near the edge. Two focusing systems were chosen as the angular profile of the incident light is position dependent. The function and condition set of the collimation system remains the same in contrast, namely to collimate the beam as much as possible. Not shown in figure 2 but present in the devices are additional air bridges that connect the top air gap, with the bottom air gap and the fiber-channel. This connection forms an escape/evaporation path for liquids during fabrication.

2.2 Parabolic Mirror

The free propagation zone inside the liquid filled microchamber lacks lateral confinement, resulting in high dispersive losses. One way to capture as much light as possible is to use parabolic mirrors as an additional lens element to focus the light into the output channel.

The parabolic mirrors are designed under the assumption of a perfect collimated beam exiting the collimation lens system. The focal point of the parabolic mirror coincides with the output channel fiber entrance. The function of the parabolic mirror is given in equation **??**. The mirror is designed under the assumption that the focal point position is chosen. This distance entails collimation lens-to-mirror (variable b) and the mirror-to-output channel distances. Equations 3 and 4 then directly relate the focal point position to the parabolic variables a and b. The developed model was parameterized to contain ray dispersion information and TIR checks across the mirror position in order to optimize the mirror function.

$$F_{parabola} = a(x - f_x)^2 + b \tag{3}$$

$$f_y = b + \frac{1}{4a} \tag{4}$$

Three configurations were simulated: one with parabolic mirrors and a spline-optimized focusing lens system, one with solely parabolic mirrors and another flat mirror model as reference for the mirror performance. The simulations show that while the output power of channel 1 is the largest for the flat mirror model, it declines more rapidly than the lensless parabolic mirrors. The system that included the focusing lenses performed worse as the ray profile incident on the lenses differs substantially from the flat mirror case for which it is was optimized.

2.3 Multiple Path Photonic Chip (MPPC) Incorporation

The applications of the employed PDMS technology cover many fields, mainly focused on rapid, low cost and low sample volume analysis of patient's serum. The previously developed multiple path photonic lab on chip (MPPC) specializes in concentration detection of analytes. The detection method is highly accurate through the parallelization of absorbance measurements, albeit quite slow. The optical fibers need to be inserted and removed into each channel for every single measurement. Considering reference measurements, the total measurement time quickly becomes too much for wide-scale application of the design. The envisioned optical router of this work provides a unique possibility of integrating channel selectivity and remaining compatible with the low-cost platform.

Figure 3 shows the envisioned chip design of the MPPC and the optical router. Additionally, a waveguide converger is added on the other side to merge the signals into one output. The routers offer the benefit of selectively outputting each channel, while the beam converger reduces the complexity on the microfluidics. On the bottom right side, the input fiber is inserted and connected to the light source, while on the top side, the output fiber is connected to a spectrometer. This design thus allows the optics to be fixed during multiple sequential measurements, which decreases the measurement time significantly.

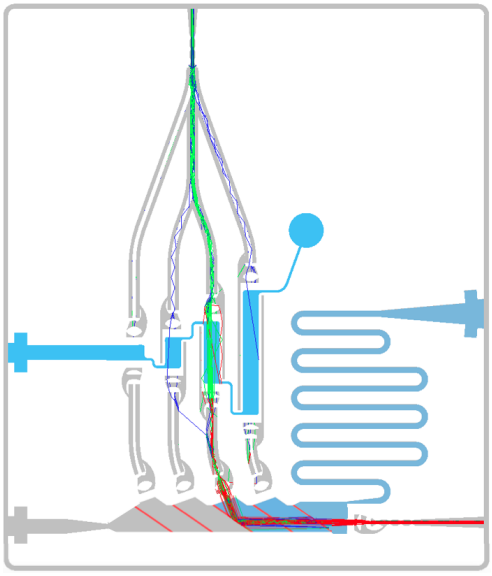

Fig. 3 *The pressure driven router incorporated into multiple path photonic lab, designed for rapid parallel sample analysis. The router sequentially screens samples of different length, while the Beam-converger brings the signal into a signal output, connected to a spectrometer.*

3 Methods & Materials

3.1 Fabrication

To produce a low-cost system, low-cost materials are required, such as soda-lime or Pyrex glass, silicon substrates and SU-8 for the master and PDMS for the device. Starting from a four-inch silicon wafer, a thermal oxidation step is done, resulting in a uniform 400 nm silicon oxide layer. However, additional steps are required as the adhesion of the SU-8 is suboptimal. Therefore, an SU-8 seed layer is added before the master is made in subsequent layers. To ensure proper adhesion of the seed layer itself, an eighteen seconds O_2 plasma activation step at 500 watts is done on the thermal oxide of the silicon wafer. The SU-8 seed layer (2005) is then applied to the wafer at 2400 rpm for 30 seconds, totaling a thickness of 5 μm. Following this, the seed layer planarizes on the wafer for 5 minutes in a closed environment. Afterwards, in open environment, the system is soft-baked near the glass transition point to initiate cross-linking from 65 °to 95 °in a 10 minute ramp-up period, with a thirty-minute cool-down period. Next, the seed layer is exposed, without a mask. A post exposure bake reduces the mechanical stress of the seed layer.

Before the SU-8 of the master is applied, an additional plasma activation step is done. The SU-8 is then applied on top of the seed layer and depending on the rotation speed of the spinner, different thicknesses can be obtained of the SU-8 layer. The O_2 plasma treatment reduces this issue. A similar soft bake as previously detailed evaporates the solvents in the SU-8. The mask is then ready for the first layer exposure in a soft contact method. Following, a PEB is done, with a one hour resting period be-

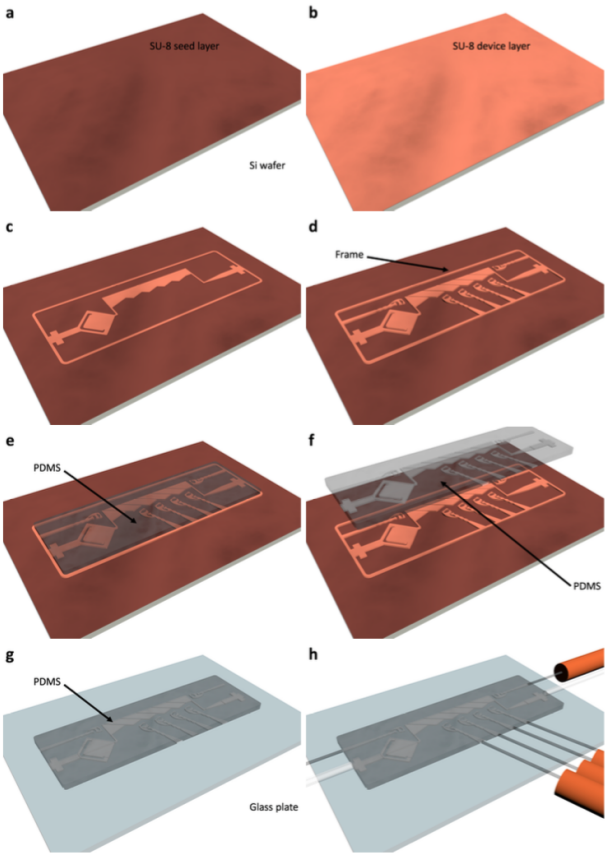

Fig. 4 *Fabrication steps of the PDMS optofluidic router.(a) 5 μm thick SU-8 seed layer. (b) spinning of the first SU-8 device layer of 10μm which defines the phaseguide gap. (c) exposure and development of the initial layer. (d) repeated steps for the optics layer and the phaseguide layer. (e) pouring of the PDMS. (f) peel-off of the PDMS device. (g) bonding of the device to a glass substrate.*

fore the master is developed in Dev-r 600. Next, a hard bake of 65°-120 °is done in one hour to remove all solvents and partially repair possible cracks. Planarization is next, where a little developed is added when the wafer rests for 15 hours (typically overnight in cleanroom conditions) to counteract swelling of the SU-8. Subsequent layers are fabricated in similar methods. After the PEB, the next SU-8 layer is applied (optics + phaseguide-mirror: 1250 rpm for 30s, phaseguide-primer: 2500 rpm 30s). To speed up the process, the overnight rest is skipped between these layers.

After the master fabrication, the devices are made by replica molding. The fabrication starts with the appropriate cleaning and dehydration steps of the substrate to ensure and optimize good adhesion of the SU-8 master. The process occurs in five steps: (1) mixing of the PDMS-polymer and curing agent in a 10:1 ratio to minimize detrimental bubble formation. (2) Pouring of the mixture over the master. (3) Curing the mixture at 80Âř C for 20 minutes. (4) Peeling off the PDMS devices from the master with a tweezer. The devices are defined by a frame that functions as a hydrophobic barrier. By doing so, repeated fabrication of individual chips on a wafer is easily done. The PDMS is poured

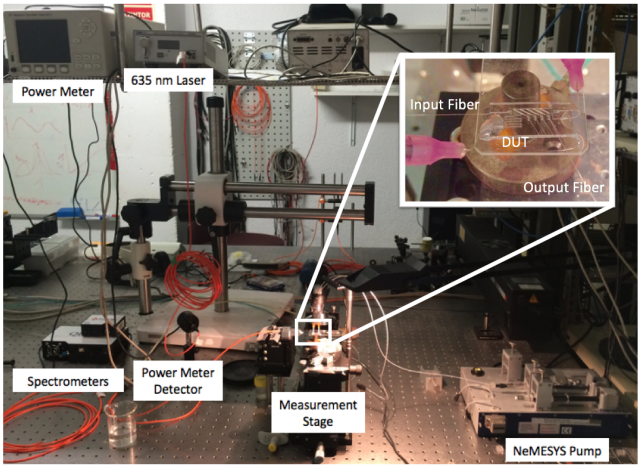

Fig. 5 *The utilized measurement setup on top of an optical workbench, consisting of two multi-axis fiber aligners, a fluidic pump (NeMESYS) and custom-made multi-fiber clamps to facilitate the fiber insertion. The inset shows a device under testing, placed on top of the vacuum chuck.*

over the device, but contained into the frame. To ease the peel-off, the frame should have no sharp edges as they introduce stresses and cracks in the PDMS/ (5) Bonding of the PDMS with a soda-lime glass plate. Before the bonding occurs, both surfaces of the PDMS and the glass plate are activated with an oxygen plasma step.

3.2 Measurement Set-Up

For the characterization of the router, a custom optofluidical set-up has been constructed. The set-up comprises out of two tri-axis stages to accommodate the input fiber and the fluidic connections. A secondary quad-axis (+ Yaw) stage aligns the output fiber to the device output ports. Custom-made fiber clamps fixate the fibers in the correct position. The 0.22 NA optical fibers (Thorlabs model AFS105/125Y) are stripped, cleaved and inserted into the channels with the aid of a droplet of ethanol. The liquid facilitates the insertion, but does not interfere with the measurement as it dries up quickly due to its high evaporation rate. The FC/PC-connected fibers are connected to Newport 1931-C power meter for optical analysis. Multi-port analysis is done by connecting OceanOptics spectrometers (OceanOptics: flame & QEPro) through intermediary APC/PC fibers. A NeMESYS pump is used as the fluidic driver, with 2.5 ml Hamilton, gas-sealed syringes connected. To speed up the measurement processes, a Labview virtual interface (VI) has been developed to synchronize the Newport power meter to the NeMESYS pump. As a result, high fluidic flow rates can be applied to align the liquid-air interface to the beginning of the initial channel. When a desired threshold in optical power is crossed, the pump stops, and re-tracts the liquid a desired amount of μl, ready for subsequent measurements of different flow profiles. Another developed VI captures multiple spectrometers at multiple desired wavelengths for targeted measurements and therefore speed up the data mining process.

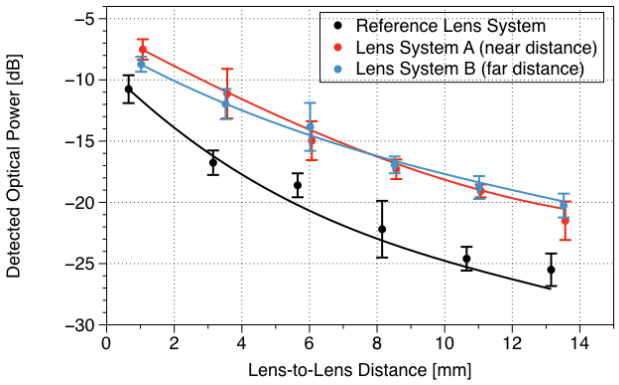

Fig. 6 *The performance of the spline optimized lens systems in terms of collected optical power versus propagation distance. A comparison is made with the previously employed lens system in black. A clear improvement between 3-6 dB is noticeable for both the short and far configurations. Each measurement point consists of between 5-7 individual measurements. The TracePro simulations are normalized against the shortest distance and matches the measurements adequately.*

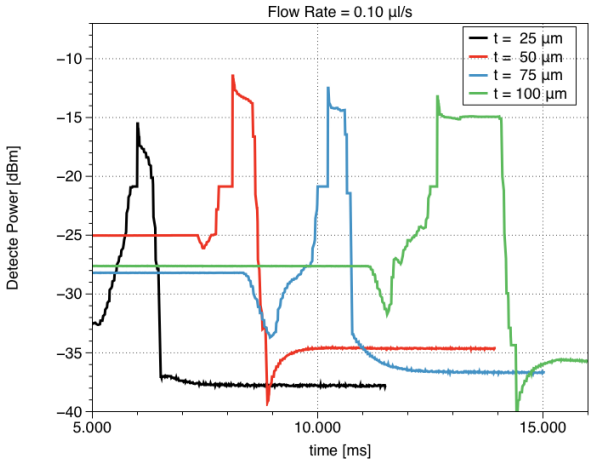

Fig. 7 *The influence of the phaseguide mirror thickness on the channel allocation performance. The very thin, high aspect ratio devices have a high distortion. As the phaseguide thickness increases, the signal becomes more stable at a cost of additional loss. Air bubbles prevented from smooth signal cross-talk.*

4 Results and discussion

4.1 Spline Optimized Lenses

The measurement results are shown in figure 6 along with the simulation results of the lens systems in TracePro. The results in black are from the previously employed lens system, which was used both as collimation and focusing system. The measurements were performed at 635 nm, with a laser power of 0.75 mW (measured output of -1.745 dBm). The measurements were referenced against this input power and the results are shown in dB loss from this reference. Each data point represents the average out of 5-7 individual measurements with a single standard deviation error bar. The devices for the lens characterization were made from three different wafers. The measurements thus incorporate fabrication variability.

The results show a clear 3 to 6 dB improvement over the previously employed system. With the size reduction of the new lens systems, the propagation distance is expressed from the last air gap of the collimation system to the first air gap of the focusing system. On contrast, the devices were normalized against fiber position, hence there is a small difference between the lateral positions of the data points for each configuration. The data also shows also a good match with the TracePro simulations, which are normalized against the first data point. While the simulations were discrete, a cubic fit was done to obtain the functions in figure 6. The simulations predict the transition point between the far and near focusing configurations accurately and gives a good representation of the dispersive losses over distance.

Quantitative measurements, similar to Muller[12] confirm a reduction of numerical aperture exiting the collimation system. The dispersion angle in PDMS is reduced from 6.75 to 4.40 °.

4.2 Pressure Driven Router

4.2.1 Mirror Performance & Repeatability

The phaseguide based switching mechanism operates on pressure driven threshold barriers. The high aspect ratio phaseguides were designed and tested to evaluate the influence of the liquid pressure on the mirror orientation. Four configurations were made: 25-50-75-100 μm. The measurement results are shown in figure 7. A trend of more stable performance is visible for the thicker configurations, albeit at a cost of additional loss. The stability of the signal decreases for the higher aspect ratio. It is expected that the liquid pushes and bends the PDMS mirror before overflow occurs. Hence, the gradual decline is visible for the 50 μm and also slightly for the 75 μm configuration. Although unclear, this can also be the reason for the distorted signal of of the 25 μm configuration as the mechanical rigidity is simply too little. The additional 1-2 dB loss from 50 μm to 100 μm configurations is related to the beam spread: for thicker phaseguides, the front and backside Fresnel reflections are more spatially separated.

4.2.2 Switching Frequency & Channel Duration

There are two components regarding the often called switching frequency: the rise and fall time/behavior upon switching channels and the channel allocation duration. Figure 8 shows the results of multiple measurements of a single channel output at different flow rates. As the slopes are exactly the same, it is clear that the rise and fall times of the channel allocation do not depend on the flow rate. It is thought that variations in the rise and fall times between different designs indicate the dependency on the gap height of the router instead of the flow rate. However, the duration of the channel allocation during the sequential switching does depend on the flow rate. Typical flow rates used in the experiments vary from 0.025 to 0.25 μl / s.

Table 1 shows the averages pulse duration from multiple measurements on a single device. The mean and variance are cal-

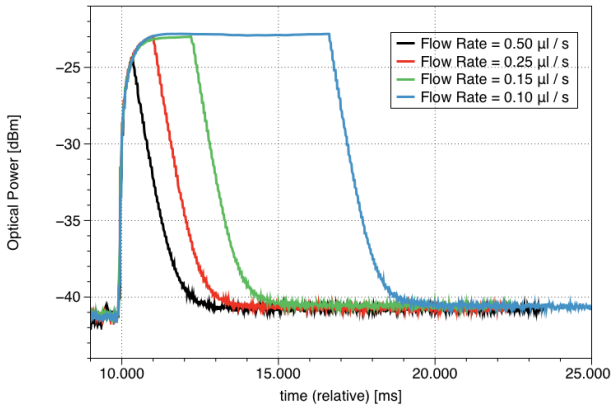

Fig. 8 *Pulse duration in function of different flow rates. The rise and fall times during switching are independent of the flow rate (same slope). The channel allocation time does depend on the flow rate.*

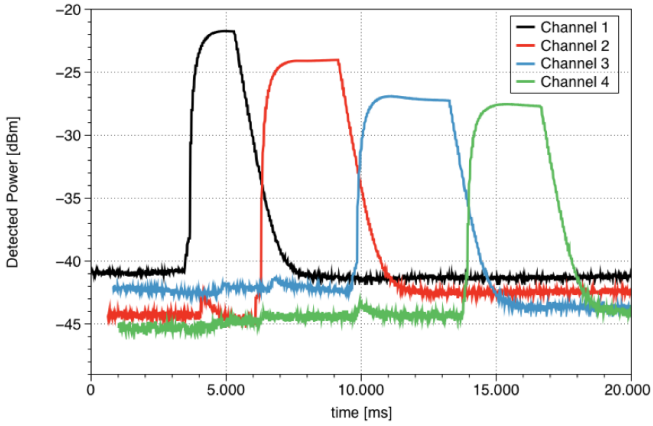

Fig. 9 *Time-aligned channel allocation of the pressure driven router. A channel-to-channel decrease of 5.81 dBm is measured.*

culated from five to seven measurements, with an approximate variance of 5 to 20 %. There is a clear inverse relation between the duration and the flow rate, which is also visible in figure 8. The pulse duration can thus vary depending on the flow rate and ranges between 0.07 ± 0.025 and 4 ± 2 Hz realistically in terms or repeatability. At higher flow rates, the risk of punch-through and leakage increases significantly. Details on the duration variances can be found in the supporting information.

Flow Rate [μl/s]	Ch1	Ch2	Ch3	Ch4
0.025	14219.6	12033.5	13275.25	5605.5
0.050	5926	8008	4132.5	2128.6
0.100	2277	1913.8	1790.8	783.2
0.150	1198.83	1048.75	864	427.4
0.200	712.17	568.6	449.2	220
0.250	544.33	294.2	287.6	150

Table 1 Average channel allocation time during router operation at different flow rates, based on 5-7 sequential measurements.

4.2.3 Insertion Loss & Cross-talk

The fluidically controlled router operates as a 1 to 4 router, where the light couples sequentially into four channels. An overview of the total device performance in terms of insertion loss and cross-talk is shown in figure 9. To understand the figure, it is important to note that the environmental noise figure (RMS) in the lab is -45.86 dBm over 1 minute measurements with all light sources shut off or reduced to the minimum. The 635nm laser power is set at 3.69 dBm. The measured device in figure 9 is a flat mirror model with the spline-optimized lenses incorporated. The flow rate was kept at 0.10 $\mu l/s$ for all channel measurements. The peak channel power is -21.73 dBm for the first channel, with a 5.81 dB decrease towards the fourth channel. Considering the laser power and the reference lens measurements, it is clear that the transition from PDMS to the switching liquid is highly reflective and dispersive. In contrast to the lens measurements, an additional 8 dB loss is measured, resulting in an insertion loss (IL) of 25.42 dB. Here, IL is defined from laser power to channel 1 output power. Regarding the static noise level, and its similar channel-to-channel decrease as the peak power, the cross-talk levels are around 20 dB, depending on the channel. This forms the basis of a high quality operating router, where the transition is an order of magnitude better than those presented in the EWOD technology[12]. This device has fast and continuous switching with smooth transitions between each channel. As a result, the dynamicac noise levels are low, peaking only around 1 to 2 dBm above their static value.

Concerning the parabolic mirror, only the lensless parabolic mirror application is characterized. The insertion loss of this device was considerably lower at 17.34 dB, with the channel 1 output power at -13.65 dBm. The normalized results are shown in table 2. At this point, it is unclear whether the lower insertion loss is directly related to the parabolic mirror as the full comparison with the flat mirror model is not completed due to measurement issues concerning air bubbles inside the router. The absence of the focusing lens system (in the lensless parabolic system) and the lack of accompanying Fresnel reflection losses can explain the improved insertion loss. The reduced channel-to-channel loss is in correspondence with the TracePro simulations and is thought to be directly related to the parabolic mirror configuration.

$P_{i,j}/P_{1,1}$ [dB]	Ch1 ON	Ch2 ON	Ch3 ON	Ch4 ON
Ch1 output [dBm]	-0.00	-20.77*	-20.51*	-20.40*
Ch2 output [dBm]	-26.17	-0.51	-20.91*	-34.37*
Ch3 output [dBm]	-27.64	-27.13	-2.18	-36.67*
Ch4 output [dBm]	-28.70	-28.27	-26.87	-2.38

Table 2 Relative cross-talk levels, normalized against channel 1 output for the lensless parabolic mirror router. (* indicates relatively unstable power level due to large dynamic noise contribution in this specific address.)

4.3 Continuous Flow Router

FDTD simulations of the dynamics of the switching liquid were outside the scope of this work. An iterative approach has been opted. The initial devices however had performance problems

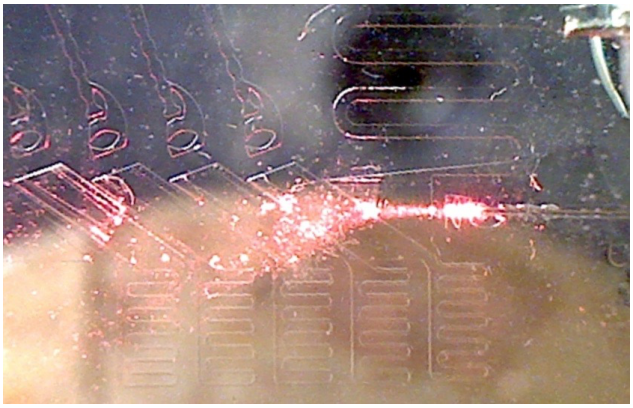

Fig. 10 *Measurement issues resulting from air bubbles formed by premature liquid overflow over the priming phaseguides. The bubbles are in the optical path and destroys the operation of the single-mirror router.*

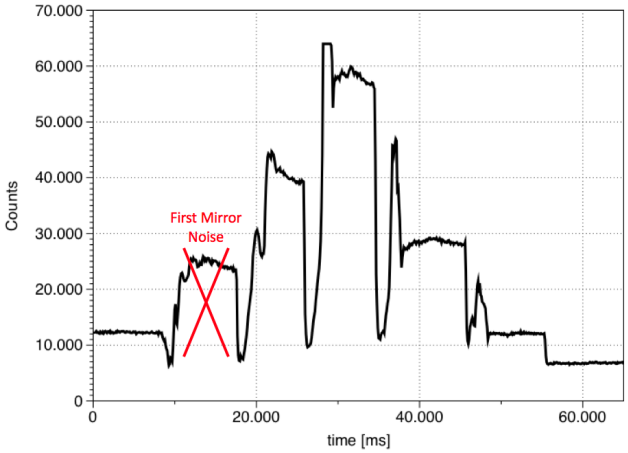

Fig. 11 *Reference measurement of H_2O in the multiple path parallel sample analysis application. The sequential channel signals are visible, proving the viability of this method. Further optimizations are required to improve the signal-to-noise ratio and the distribute the power per channel equally.*

due to fluidic behavior. Firstly, additional phaseguides were added as primers (130 μm gap, 20 μm barrier height). These were however insufficient to control the liquid towards back-side wetting of the mirrors.

Next, the continuous flow router was developed, initially also with these primer phaseguides. The primer specification was targeted at 200 μm to compensate the initial problem. Due to fabrication errors, the layer was not according to specification and remained at 20 μm. The initial problems remained, and are depicted in figure 10. Again, premature overflow occurred, creating air bubbles in the optical path. These are visible in both the first microchamber and subsequent microchambers at the top-side, near the output lenses. These preliminary measurements have resulted in a re-design of the continuous flow router, which was illustrated in figure 1-(b) and is pending characterization. There, the liquid follows a more natural path and is guided through back-channels instead of relying on the operation of priming phaseguides.

4.4 MPPC Integration Analysis

The integration of the router in an MPPC was completed. In this work, proof-of-principle measurement confirm the possibility of the router integration. However, further optimizations must be completed before the system can be used for concentration measurements. These obstacles are explained with the reference H_2O measurement results in figure 11. As can be seen in the figure, a seemingly first channel allocation between 10 and 20 seconds actually corresponds to the router's OFF-state, initial mirror. The alignment between this first mirror and the fiber output is coincidental. To remove this contribution, an ink-aperture is required (missing in the characterized device).

The signal-to-noise ratio is the most cumbersome issue in this device. An included ink-aperture would solve this partially by lowering the noise floor. Also, the ink aperture would reduce cross-talk levels and forms a barrier between the channels so that the sharp edges at the beginning of each channel allocation are filtered out. These is device noise that partially passes around the MPPC liquid, similar to the undesired OFF-state mirror output. With these improvements, the signal-to-noise ratio would be sufficient for channel two and possibly also for channel one. However, the signal-to-noise ratio in channel three and four remains too low, with a 3-5 dB variation from channel 2. Ideally all channels should peak at maximum count level of 60k for the flame spectrometer. For this configuration, just below the saturation level, the highest signal-to-noise ratio is obtained. This difference in peak counts between the channels is related to the total liquid path length in the device (router + MPPC), as this contributes most significantly to losses. The total liquid path length is the lowest in the second channel, and the highest in the fourth channel. The PDMS platform can not implement a gain medium to compensate for these losses. Thus the detected power difference can not be compensated by amplifying channels three and four. There are two options for improvement. One is the addition of extra losses in channel 2, in order to reduce its peak power level. This results in more equal count-levels and are raised by setting a larger integration time (100 ms in figure 11). The second option is a dynamic labview VI with the purpose of recognizing a channel switch and therefore, dynamically switching the integration time towards the corresponding value of that specific channel, in order to extract the highest signal-to-noise ratio without reaching saturation.

5 Future Work

A limitation of the presented routers can be found in the high losses due to the lack of total optical confinement (as in optical waveguides). With the use of a high RI-liquid, vertical confinement is possible. Current issues revolved around the hydrophilic-hydrophobic nature of the RI-liquid and the PDMS. When both the switching liquid and the PDMS behave similarly, the pressure barrier effect is diminished. New devices with a hydrophilic activation of the PDMS routers could make the device compatible with high RI-liquids.

Newly designed routers for the parabolic mirror comparison await characterization. The designs include: (1) air-leakage paths to reduce air bubbles, (2) increased chambers to avoid any aforementioned bubbles to be in the optical path and (3) corrugated sidewalls to pin the bubbles and thus prevent them from expanding into the optical path. Also planned is the characterization of the dual-mirror continuous flow router of figure 1-(b).

Finally, new designed MPPC systems are designed that include all of the above improvements, along with a redesigned ink-aperture and an adjusted channel power distribution to obtain high signal-to-noise ratios in all channels.

6 Conclusions

A compact, simple, miniaturized and integrable fluidically controlled optical router has been built using soft-lithographic techniques. The router is made entirely of PDMS and air ensuring low-cost and robustness. The recently developed microfluidic phaseguides have been exploited to create the PDMS optical mirrors.

Repetitive power measurements are obtained, along with and channel frequencies (the inverse of the allocation duration) varying between 0.07 ± 0.025 and 4 ± 2 Hz. Typical insertion loss figures varied between devices, from 17.34 to 25.42 dB. The channel-to-channel decrease in power differs between flat mirror routers (5.81 dB measured) and those included with lensless parabolic mirrors at just a 2.38 dB decrease. The cross-talk levels for all devices and all channels is similar at around 20 dB. In terms of cross-talk and frequency flexibility, the presented router performs better than the direct EWOD competitor. Overall, the low-cost of this device ensures practical viability towards the future.

Finally, the presented router has been integrated in a previously reported MPPC for parallel sample analysis. The proof-of-principle measurements confirm the viability of this concept for the future. At the moment, some obstacles remain before the device can operate as intended. The key areas of improvement have been identified and possible solutions are included into the designs of upcoming devices.

7 Acknowledgements

This work has been made possible and funded by the Centre National de Microelectrinca de Cataluyna (CNM). Also special acknowledgements to the board of the UPC-coordinated master in photonics for creating the opportunity for this project.

References

1 M. Guttierez, A. Llobera, A. Ipatov, J. Vila-Planas, S. Minguez, S. Demming, S. Buttgenback, F. Capdevila, C. Domingo and C. Jimenez-Jorquera, *Sensors (Basel, Switzerland)*, 2011, **11**, 4840–4857.

2 S. Demming, J. Vila-Planas, S. Aliasghar Zadeh, A. Edlich, E. Franco-Lara, R. Radespiel, S. Büttgenback and A. Llobare, *Electrophoresis*, 2011, 431–439.

3 I. Rodriguez-Ruiz, M. Conejero-Muriel, T. N. Ackermann, J. A. Gavira and L. Andreu, *Lab on Chip*, 2014, **15**, 1133–1139.

4 C. Dongre, J. van Weerd, N. Belline, R. Osellame, G. Cerullo, R. van Weeghel, H. J. Hoekstra and M. Pollnau, *Biomedical Optics Express*, 2010, **1**, 729–735.

5 D. Kimmel, G. LeBlanc, M. M.E. and D. Cliffel, *Analytical Chemistry*, 2012, **84**, 685–687.

6 S. Balslev, A. Jorgensen, B. Bilenberg, K. Mogensen, D. Snakenborg, O. Geschke, J. Kutter and A. Kristensen, *Lab on a Chip*, 2006, **6**, 213–217.

7 D. Lepage, J. A., J. Beauvais and J. Dubowski, *Light: Science and Applications*, 2013, **2**, year.

8 B. I. S. D. C. N. J. E. P. C. D. S. B. Jordi Vila i Planas, Elisabet Fernandez-Rosas and A. Llobera, *Nature Protocols*, 2011, **6**, 1642–1655.

9 A. Llobera, R. Wilke and S. Buttgenback, *Talanta*, 2008, **75**, 473–479.

10 J. Fouquet, Optical Fiber Communication Conference, 2000.

11 A. Groisman, S. Zamek, K. Campbell, L. Pang, U. Levy and Y. Fainman, *Optics Express*, 2008, **16**, 13499–13508.

12 P. Muller, D. Kopp, A. Llobera and H. Zappe, *Lab on a Chip*, 2013, **14**, 737–743.